Quantum computing with atomic Josephson junction arrays

Lin Tian and P. Zoller
Institute for Theoretical Physics, University of Innsbruck, A-6020 Innsbruck, Austria
(Received 12 June 2003; published 20 October 2003)

We present a quantum computing scheme with atomic Josephson junction arrays. The system consists of a small number of atoms with three internal states and trapped in a far-off-resonant optical lattice. Raman lasers provide the ''Josephson'' tunneling, and the collision interaction between atoms represent the ''capacitive'' couplings between the modes. The qubit states are collective states of the atoms with opposite persistent currents. This system is closely analogous to the superconducting flux qubit. Single-qubit quantum logic gates are performed by modulating the Raman couplings, while two-qubit gates result from a tunnel coupling between neighboring wells. Readout is achieved by tuning the Raman coupling adiabatically between the Josephson regime to the Rabi regime, followed by a detection of atoms in internal electronic states. Decoherence mechanisms are studied in detail promising a high ratio between the decoherence time and the gate operation time.

DOI: 10.1103/PhysRevA.68.042321 PACS number(s): 03.67.Lx, 03.75.Lm, 74.50.+r

I. INTRODUCTION

Josephson effects originate from a tunneling of the particles in the condensed modes between two superfluids and reflect the phase difference of the macroscopic wave functions between the superfluids. Initially discovered in the superconductors [1,2], Josephson effects have been studied intensively in trapped atoms both theoretically and experimentally [3,4]. In the atomic case, Josephson junctions can be constructed between two superfluids spatially separated by a double-well potential and can be constructed between atomic internal modes coupled by lasers. Studies include the macroscopic quantum coherence between two atomic condensates and the observation of the Josephson dynamics [5].

One important application of the Josephson junctions discussed in recent years is in quantum computing. Various superconducting Josephson devices have been proposed for implementing a quantum computer, including the charge qubit, the flux qubit, and the phase qubit. These qubits have been experimentally tested and have shown quantum coherent oscillations between macroscopically distinguishable states [6–9].

The atomic Josephson junctions can also be explored for quantum computing. In this paper, we present a candidate for implementing an atomic ''flux'' qubit with a small number of atoms in an optical trap. We assume that a Bose-Einstein condensate with three atomic states is stored in the lowest vibrational state of an optical trap [10]. The three internal atomic states correspond to three bosonic modes. Each mode is the analog of a superconducting metallic island. Raman lasers generate the Josephson links between the internal modes, while atomic collisions provide an effective capacitive couplings between the modes. The phase differences between lasers play the role of the magnetic field in the superconducting loop. With competition between the Josephson energy and the collision energy, the atoms behave collectively and the stationary states of the qubit have a coherent particle transfer—the persistent current—between the internal modes. With only 15 atoms [11], the atomic counterpart of the superconducting flux qubit [7,8] can be realized, which bears all the qualitative features of the superconducting flux qubit.

Compared with the superconducting flux qubit, the parameters of the atomic flux qubit can be controlled with large flexibility and high uniformity. Both the Josephson coupling and the collision interaction can be adjusted by external electromagnetic sources. The Josephson couplings of different junctions can be made to high accuracy with the fine control of laser. While for superconductors, not only do the junction parameters fluctuate due to the inaccuracy in fabrication, but also the parameters are fixed for one sample. This advantage makes it easier to scale up the number of qubits in the atomic systems and provides various ways to implement gate operations. Another merit of the atomic qubit is that a projective measurement can be performed by adiabatically switching the Raman couplings. On the contrary, an efficient readout for the solid-state qubits is a problem many people are studying. The drawback of the atomic qubit is the slow gate speed which is limited by the strength of the collision interaction. Meanwhile, this drawback can be compensated by the long decoherence time. In the solid-state systems, various elementary excitations can damage the coherence of the quantum states in a time that is only one order longer than the gate time; while we show that in the atomic qubit, the decoherence time is 1000 times the gate operation time.

In the following, the major results are summarized. In Sec. II, we briefly review the superconducting flux qubit and the experimental achievement for the flux qubit. In Sec. III, we give a detailed description of our proposal for the atomic flux qubit and how it can be realized experimentally. We also characterize the qubit at different parameter regimes and present typical energy scales for the qubit. Also we introduce the phase mode to compare this qubit with the superconducting one, and show that a small number of atoms indeed represent the macroscopic behavior of a Josephson junction. This section is followed by Sec. IV where the implementation of quantum logic gates is studied. In Sec. V, a projective measurement scheme is constructed via the adiabatic switching of the Josephson couplings. The decoherence of the qubit

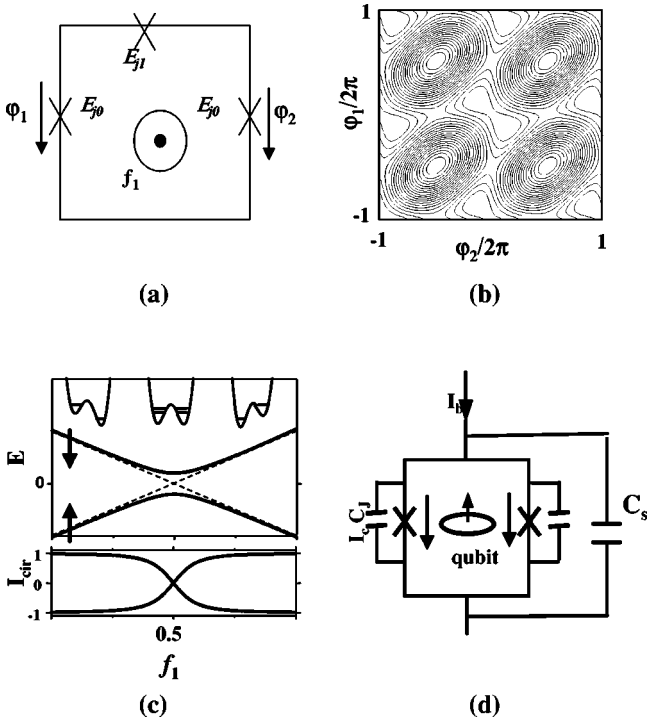

FIG. 1. The superconducting flux qubit. (a) The circuit of the flux qubit. (b) The potential energy for the qubit. The black centers are local maxima and the white centers are local minima. (c) The energy and the average current of the qubit vs the flux. The arrows indicate the qubit states with opposite currents. The double-well potentials at the corresponding flux are plotted. (d) The measurement of the qubit by a dc SQUID.

is discussed in Sec. VI. The conclusions are given in Sec. VII.

II. THE SUPERCONDUCTING FLUX QUBIT

Josephson junctions have been proved to be a promising building block for quantum computers. Various proposals of Josephson circuits at different parameter regimes have been studied [6–8]. Among these, the superconducting flux qubit—also named the persistent-current qubit—has been intensively studied both theoretically and experimentally. In the following, we summarize the basic facts of the flux qubit in superconducting Josephson junctions to allow the comparison with the atomic flux qubit introduced in the following section.

A. The circuit of the qubit

The superconducting flux qubit [7,8] is a superconducting loop with three Josephson junctions in series, as in Fig. 1(a). Written in terms of the phase differences φ_1 and φ_2, the Hamiltonian [Eq. (11) in [8]] is

$$\mathcal{H}_t=\tfrac{1}{2}\vec{P}^T\mathbf{M}^{-1}\vec{P}+E_J\{2+\alpha-\cos\varphi_1-\cos\varphi_2 - \alpha\cos(2\pi f_1+\varphi_1-\varphi_2)\}, \quad (1)$$

where $\vec{P}=(\hat{P}_1,\hat{P}_2)^T$ are the conjugates of the phase variables and have the physical meaning of the charges on the islands. The first term is the capacitive energy with $\mathbf{M}=(\hbar/2e)^2\mathbf{C}$, where $\mathbf{C}$ is the capacitance matrix of the circuit. The rest of the terms form the Josephson energy with $E_J=I_c(\hbar/2e)^2$ and I_c being the critical current of the junctions. The third junction at the top of the circuit has a Josephson energy of αE_J, with $\alpha=0.75$. The magnetic flux in the loop, f_1, in unit of the flux quantum $\Phi_0=\hbar/2e$ is an important control parameter for the qubit. Both the stationary states and the one-bit logic gates are controlled via this flux.

The Hamiltonian in Eq. (1) describes a phase particle in a two-dimensional periodic potential as is shown in Fig. 1(b). Each unit cell has two energy minima and is a double-well potential. At $f_1=0.495$, the lowest two states of the qubit localize in one of the two wells, respectively, and have opposite circulating currents. At $f_1=1/2$, the lowest two states are symmetric and antisymmetric superpositions of the localized flux states, and the energy splitting is due to the tunneling of the flux states over the potential barrier. Considering only the lowest states, the qubit can be described by the Pauli matrices for a 1/2 spin: $\mathcal{H}_q=(\epsilon_0/2)\sigma_z+(t_0/2)\sigma_x$, where the eigenstates of σ_z are the localized flux states and ϵ_0 varies linearly with $(f_1-1/2)$. Typically, the Josephson energy is $E_J=200$ GHz and $E_J/E_C=80$. Numerical calculations of the energy and current are shown in Fig. 1(c). The energy difference of the qubit states at $f_1=0.495$ is $\omega_q\sim 10$ GHz with the average currents of $\pm 0.7I_c$ at $f_1=1/2$, $t_0=10$ GHz.

For a quantum circuit to be a good qubit for fault-tolerant quantum computing, five requirements have to be met [12]: (1) to identify a scalable quantum system; (2) to perform universal quantum logic gates; (3) to prepare the initial state; (4) to read out the qubit states; and (5) to have a decoherence time longer than 10^4 quantum operations. The three-junction loop behaves as an effective two-level system and can be mapped onto a 1/2 spin. The qubit can be prepared to the ground state by cooling it to a temperature of $T\sim 50$ mK $\ll\omega_q$.

B. Quantum logic gates

To achieve universal quantum logic operations, two elementary gates are required: single-qubit rotation and two-qubit controlled gate. For the superconducting flux qubit, the single-qubit gate is achieved by applying microwave oscillations to the superconducting loop. Typically, the Rabi frequency is $\omega_r=10$–100 MHz in proportion to the amplitude of the microwave. The two-qubit gate is constructed via the coupling of the circulating currents of the two qubits: $\mathcal{H}_{int}=M_{12}|\langle I_1\rangle\langle I_2\rangle|$ with $I_{1,2}$ being the currents of the two qubits and M_{12} being the mutual inductance. The interaction can be of order of 1 GHz.

C. Qubit state readout

The qubit is measured by inductively coupling the qubit to a dc superconducting quantum interference device (SQUID) magnetometer which is a superconducting loop

with two Josephson junctions as is shown in Fig. 1(d). When the current that flows through the SQUID increases, the SQUID stays in the superconducting state until a critical current I_c^{eff} is reached, where the SQUID makes a transition to a finite voltage state. The critical current is varied by the flux generated by the qubit: $\delta I_c^{eff} = \pm \delta\varphi_q I_c^{sq} \sin \pi f_{ex}$, where f_{ex} is the external flux in the SQUID and $\pm \delta\varphi_q$ are flux of the two qubit-states respectively. By measuring the critical current, the qubit states are read out. Due to fluctuations, the measured critical current has a distribution that is wider than δI_c^{eff} which results in a nonprojective measurement of the qubit.

D. Decoherence

Many factors can result in quantum errors against the superconducting qubits. First, the errors can come from the imperfect control of the qubit circuits, for example, off-resonant transitions during gate operations and unwanted dipolar couplings between qubits. These errors can be prevented by the quantum control approach. Second, the fluctuations of the environment of the qubit can cause decoherence of the qubit. In the solid-state qubits, many elementary excitations exist that can damage the qubit state, including the dipolar interactions between the qubit and the nuclear spins, the background charge fluctuations, and the noise coupled to the qubit from the measurement circuits. The decoherence time measured in experiments is 100 nsec [9], which is about ten times the operation time. This gives a lower bound for the generic decoherence of the qubit.

III. THE ATOMIC FLUX QUBIT

In this section we present an atomic counterpart of the superconducting flux qubit. The qubit is made of a mesoscopic Bose-Einstein condensate of three-level atoms trapped in the lowest motional states of an optical trap and interacting with each other via cold collision. Josephson junctions, which are the building blocks of this qubit, are constructed by laser coupling of the three bosonic modes of the trapped atoms.

A. The physical system and the Hamiltonian

We consider a small number of three-level atoms trapped in a one-dimensional (1D) optical lattice, as shown in Fig. 2(a). The corresponding Hamiltonian is

$$\mathcal{H}_0 = \sum_\alpha \int d\vec{x}\, \psi_\alpha^\dagger(\vec{x}) \left(-\frac{\hbar^2}{2m}\nabla^2 + V(\vec{x}) \right) \psi_\alpha(\vec{x}) + \sum_{\alpha,\beta} U_{\alpha\beta\beta'\alpha'} \int d\vec{x} \psi_\alpha^\dagger(\vec{x}) \psi_\beta^\dagger(\vec{x}) \psi_{\beta'}(\vec{x}) \psi_{\alpha'}(\vec{x}) - \sum_{\alpha\neq\beta} \int d\vec{x} [T_{\alpha\beta}(\vec{x}) \psi_\alpha^\dagger(\vec{x}) \psi_\beta(\vec{x}) + \text{H.c.}], \quad (2)$$

where the three internal states are labeled by α, β, and m is the mass of atoms.

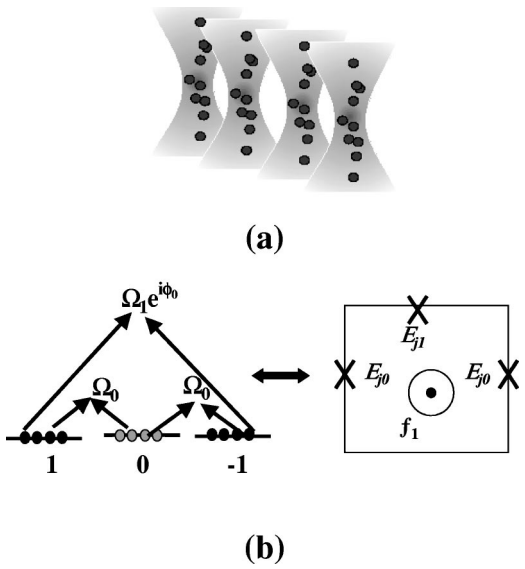

FIG. 2. The atomic Josephson junction qubit. (a) Atoms trapped in the cigar-shaped optical potential by laser beams. (b) Left: the internal modes coupled by Raman pulses. Right: the superconducting flux qubit.

The first term in Eq. (2) is the single-particle energy in a harmonic trapping potential, $V(\vec{x}) = \frac{1}{2} m \omega_\parallel^2 x^2 + \frac{1}{2} m \omega_\perp^2 (y^2 + z^2)$, where $\omega_{\perp,\parallel}$ are the trapping frequencies in the transversal direction and the longitudinal direction, respectively. In particular, we choose a cigar-shaped geometry, $\omega_\perp \gg \omega_\parallel$. The second term in Eq. (2) is the collisional interaction. We choose for the three internal atomic states the hyperfine levels $F=1$, $M_F = 0, \pm 1$. In this case the interaction has the form $U = c_2 \vec{F}_1 \cdot \vec{F}_2$, with $\vec{F}_i$ being the angular momentum of the atoms. Here, $c_2 = (g_2 - g_0)/3$ with $g_F = 4\pi\hbar^2 a_s^{(F)}/m$, where $a_s^{(F)}$ is the s-wave scattering length in the channel of total angular momentum F [13,14]. The last term in Eq. (2) is the Josephson couplings between the internal states generated by Raman transitions. Both the amplitudes and the phases of these couplings can be accurately controlled by adjusting the laser parameters.

We assume the trapping frequencies to be much larger than all the other relevant time scales (e.g., the qubit energy and the gate speed) so that the atoms stay in the motional ground states and the qubit can be described by a three-mode Hamiltonian

$$\mathcal{H}_0 = U_0[(\hat{N}_1 - \hat{N}_{-1})^2 + (2\hat{N}_0 - 1)(\hat{N}_1 + \hat{N}_{-1})] + 2U_0(\hat{a}_1^\dagger \hat{a}_{-1}^\dagger \hat{a}_0^2 + \text{H.c.}) - \sum_{\langle\alpha,\beta\rangle} (\Omega_{\alpha\beta} \hat{a}_\alpha^\dagger \hat{a}_\beta + \Omega_{\alpha\beta}^* \hat{a}_\beta^\dagger \hat{a}_\alpha), \quad (3)$$

where $\hat{N}_\alpha$ is the number operator for the mode α. The second line in this Hamiltonian gives a particle flow term where two atoms in the state $M_F = 0$ collide to form an atom in the states $M_F = +1$ and $M_F = -1$. The interaction strength is

$$U_0=\frac{4\pi\hbar^2(a_s^{(2)}-a_s^{(0)})}{3m}\int d^3\vec{x}|\phi(\vec{x})|^4, \tag{4}$$

where $\phi(\vec{x})$ is the motional ground state of the trapping potential. With a fixed number of atoms, the interaction strength increases with the density of the atoms. The Josephson tunnelings are given by

$$\Omega_{\alpha\beta}=\int d^3\vec{x}\,T_{\alpha\beta}(\vec{x})|\phi(\vec{x})|^2. \tag{5}$$

Specifically, we assume $\Omega_{-1,0}=\Omega_{0,1}=\Omega_0$ and $\Omega_{-1,1}=\Omega_1 e^{i\phi_0}$, as shown in Fig. 2(b), where Ω_1/Ω_0 ranges between 0.5 and 1.5, and is an important factor for maximizing the speed of the gate operations. The phase ϕ_0 is the analog of the magnetic flux f_1 of the superconducting qubit and is an effective controlling knob for the quantum logic gates.

The basis element in this qubit is to construct atomic Josephson junctions with a small number of atoms. The atomic Josephson junctions have three distinct parameter regimes [3]: (1) the Fock regime with $U_0\gg\Omega_0 N_t$; (2) the Josephson regime with $U_0N_t^2\gg\Omega_0N_t\gg U_0$; and (3) the Rabi regime with $\Omega_0N_t\gg U_0N_t^2$. In the Fock regime, the collision energy dominates over the Josephson couplings. In the Josephson regime, the qubit behaves as a phase particle in the Josephson potential energy. In the Rabi regime, the atoms behave as noninteracting particles described only by the Josephson couplings. In a superconducting Josephson junction, the Rabi regime can never be approached with the enormous number of Cooper pairs. While for the atomic Josephson junctions, all three regimes are possible. In this paper, we assume a mesoscopic number of atomic qubits in the Josephson regime. When compared with a large ensemble of atoms (say 10^5 atoms) in a superfluid state where the three-mode approximation becomes inaccurate during fast gate operation, this system has the advantage that the three-mode model is robust against the qubit dynamics.

In the Josephson regime, with $N_t\gg1$, Eq. (3) can be approximated by a phase model [3]. We introduce the phase variables $\varphi_{-1,1}$ that are the conjugate operators of the number operators $\hat{N}_{-1,1}$, respectively. Due to particle number conservation, $\hat{N}_0$ is not an independent operator with $\hat{N}_0=N_t-\hat{N}_{-1}-\hat{N}_1$. Omitting the term $\hat{a}_1^\dagger\hat{a}_{-1}^\dagger\hat{a}_0^2$ [15] and neglecting the terms of order $1/\sqrt{N_t}$, the Hamiltonian is

$$\mathcal{H}_{phase}=\tfrac{1}{2}|U_0|\vec{P}^T\mathbf{M}^{-1}\vec{P}-\tfrac{2}{3}N_t\Omega_0(\cos\varphi_1+\cos\varphi_{-1})-\tfrac{2}{3}N_t\Omega_1\cos(\varphi_1-\varphi_{-1}+\phi_0), \tag{6}$$

where $\vec{P}=[\hat{N}_1-N_t/8,\hat{N}_{-1}-3N_t/8]^T$ and $M_{1,1}=M_{-1,-1}=1$, $M_{1,-1}=-3$. This shows that with a large number of atoms in the qubit, the major part of the Hamiltonian maps to Eq. (1) of the superconducting flux qubit with $E_c=3|U_0|/4$, $E_J=2\Omega_0N_t/3$. In the following section, we will discuss the validity of the phase model for a comparatively small number of atoms.

We illustrate our model with the following parameters for $N=15$ sodium atoms in the trap. For ^{23}Na, we choose the trap size to be $L_\parallel=0.85$ μm and $L_\parallel=10L_\perp$, which can be achieved with a far red detuned laser. The trapping frequencies are $\omega_0^\parallel=3.7$ kHz and $\omega_0^\perp=370$ kHz. Let $a_s^{(2)}-a_s^{(0)}=-30$ nm. With a density of $\rho=3\times10^{14}\,\mathrm{cm}^{-3}$, the collision interaction is $U_0=550$ Hz. The Josephson couplings can be controlled so that $\Omega_{\alpha\beta}\sqrt{N_\alpha N_\beta}\gg U_0$ in analogy to the superconducting flux qubit. We let $2\Omega_0\langle N_\alpha\rangle\approx110U_0$ and $\Omega_1/\Omega_0=0.8$ in the following calculations. In the notations of the superconducting qubit, $E_J/E_c\approx130$.

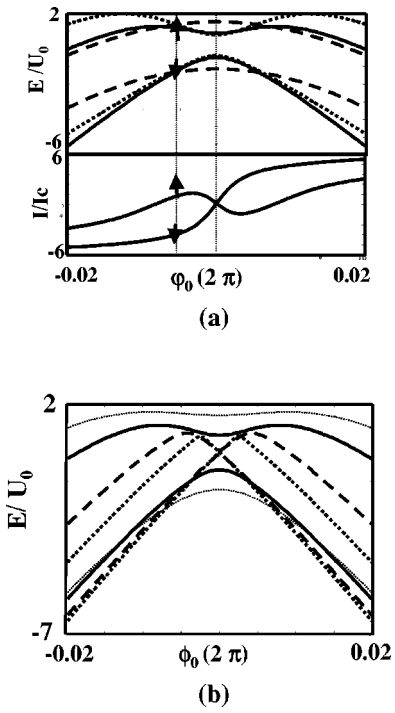

FIG. 3. The energy and average current of the qubit states vs the phase ϕ_0. (a) $N_t=15$ atoms. Solid lines, $U_0=550$ Hz; dashed lines, $U_0=0$; and dotted lines, for the symmetric interaction with $\overline{U_1}=550$ Hz. (b) Energies of the qubit with various numbers of atoms. Solid lines, $N_t=15$; thin dotted lines, $N_t=10$; dashed lines, $N_t=30$; and dotted lines, $N_t=50$.

B. Effective two-level system

We have numerically studied the Hamiltonian in Eq. (3) with the above parameters. In Fig. 3(a), we plot the energies and the average currents of the eigenstates of the qubit versus the phase ϕ_0 in the range 0.48–0.52 (in unit of 2π). It is shown that with $c_2<0$, the energy spectrum of the qubit has the same butterfly shape as that of the superconducting qubit in Fig. 1(c). We define the lowest two states as the effective two-level system of a qubit. At $\phi_0=0.495$, the qubit energy is $\omega_q=1.3$ kHz, where the states are labeled by the arrows. The stationary states have a coherent transfer of the atoms between the internal states, which provides a persistent particle current for the qubit, where the current operator is defined as $\hat{I}_{1,0}=i\Omega_0(\hat{a}_1^\dagger\hat{a}_0-\hat{a}_0^\dagger\hat{a}_1)$. The currents of the two-qubit states flow in opposite directions just as in the superconducting qubit, with $|\langle I_{1,0}\rangle_1-\langle I_{1,0}\rangle_2|=4.6\Omega_0$. This shows that the atoms behave collectively just as the electrons

in the superconducting wires, which is a result of the interaction between the atoms. For comparison, the energies of the qubit when $U_0=0$ are also plotted as the dashed lines in Fig. 3(a).

At $\phi_0=1/2$, the energy splitting $t_0=750$ Hz, which is the counterpart of the quantum tunneling in the flux qubit and an important feature of the qubit that is crucial for the gate operations. We studied this splitting with various circuit parameters. Our result shows a dramatic dependence of t_0 on the ratio between the Josephson couplings $r_0=\Omega_1/\Omega_0$: at $r_0=0.75$, $t_0=1.25$ kHz, at $r_0=1$, $t_0=0.1$ Hz, and for $r_0>1$, t_0 is almost unchanged as r_0 increases.

It can be shown that the detailed form of the interaction does not change the main features of the qubit. For example, with a symmetric interaction $U=U_1\Sigma\hat{N}_\alpha^2+U_2(\hat{N}_1\hat{N}_{-1}+\hat{N}_1\hat{N}_0+\hat{N}_{-1}\hat{N}_0)$, the main physical properties of the qubit are well preserved. The energy spectrum with this interaction is plotted as dotted lines in Fig. 3(a), where we choose the interaction to be $U_1-U_2/2=-U_0$ with $\Omega_1/\Omega_0=0.75$. Note that the effect of the collisions between different modes only renormalizes the interaction U_1 and the interaction is equivalent to $U=\overline{U}_1\Sigma\hat{N}_\alpha^2$ with $\overline{U}_1=U_1-U_2/2$.

C. "Finite-size" effect

To see the effect of the small number of the atoms, we calculate the energies with various numbers of atoms, as is shown in Fig. 3(b). The plot shows that the energies of the qubit converge as the number of atoms increases. Furthermore, it shows that when $N_t=15$ the states of the qubit well represents the key features of a superconducting flux qubit—the features of a qubit in the phase model. The surprising fact is that with a small number of atoms, the atomic qubit reflects the properties of the flux qubit with over 10^{10} Cooper pairs: the qubit states have opposite persistent currents; the phase in the Raman coupling induces energy difference that is nearly linear with $\phi_0-1/2$; besides, even the wave functions in the phase space can be described by the localized phase states.

The wave function in the basis of the phase variables is $|\psi\rangle=\int d\varphi_1 d\varphi_{-1}|\varphi_1,\varphi_{-1}\rangle\langle\varphi_1,\varphi_{-1}|\psi\rangle$. In our calculation, we use the number state basis for the states: $|\psi\rangle=\Sigma_{n_1,n_{-1}}c_{n_1,n_{-1}}|n_1,n_{-1}\rangle$, where $c_{n_1,n_{-1}}$ is the coefficient of the wave function. The wave function in the phase basis is then $\langle\varphi_1,\varphi_{-1}|\psi\rangle=\Sigma_{n_1,n_{-1}}c_{n_1,n_{-1}}e^{-i\varphi_1 n_1-i\varphi_{-1}n_{-1}}$. In Fig. 4, $|\langle\varphi_1,\varphi_{-1}|\psi\rangle|^2$ of the ground state is plotted in the phase basis with $N_t=15$, 30, and 60.

The phase model predicts that at $\phi_0=1/2$ the wave function to be a superposition of two local flux states. For the small number of atoms with a weak interaction, Fig. 4(a) shows that the qubit state localizes at the center of the phase-space in contrast to the phase-model prediction, while, with $N_t=60$, the state is a superposition of two local states in agreement with that of the phase model. Figure 4(c) shows the same result for $\phi_0=0.495$. With a stronger interaction, Figs. 4(b) and 4(d) show that the state of $N_t=15$ atoms agrees with the phase-model result. Our study indicates that the behavior of the qubit depends strongly on the factor $U_0N_t^2/\Omega_0N_t$. When $U_0N_t^2<\Omega_0N_t$, the qubit enters to the Rabi regime and single-atom behavior starts to dominate over the collective behavior. Our result also shows that with $N_t=15$ the qubit represents the main features of a phase-model qubit.

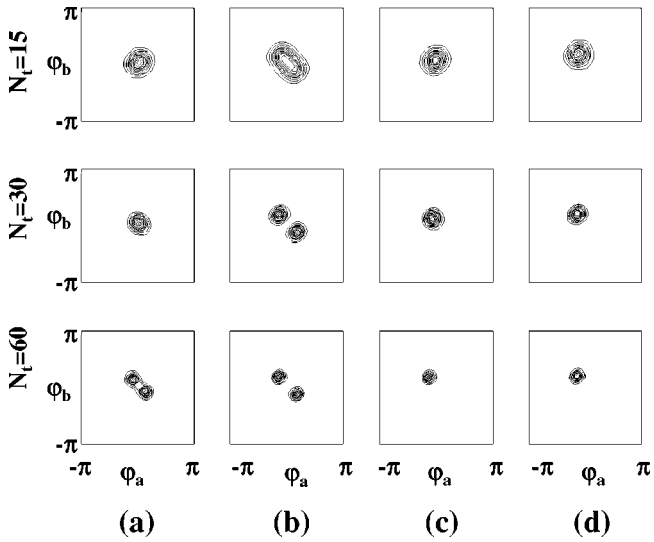

FIG. 4. Contour plots of the probability $|\psi_g(\varphi_1,\varphi_{-1})|^2$ of the ground-state wave function of the qubit: (a) $U_0=55$ Hz, $\phi_0=1/2$; (b) $U_0=1100$ Hz, $\phi_0=1/2$; (c) $U_0=55$ Hz, $\phi_0=0.495$; (d) $U_0=1100$ Hz, $\phi_0=0.495$.

IV. GATE OPERATIONS

Below, we discuss how to realize quantum logic gates, the qubit initialization, qubit state readout, and the decoherence properties of the atomic flux qubit.

A. One-bit gate

The superconducting qubit is operated with external magnetic fields where microwave pulse in resonance with the qubit frequency is radiated on the superconducting loop. Off-resonant transitions to other states of the qubit can be neglected since the Rabi frequency is much smaller than the detuning.

A similar scheme can be applied in the case of the atomic flux qubit. If we take a Raman laser coupling of any two of our bare atomic states which make up the qubit, and tune these lasers to match the energy difference of the qubit states, we can perform Rabi rotations between the states. In order not to excite any higher-lying states, the Rabi frequency should be less than the level spacings. In the atomic flux qubit, the qubit frequency and the detuning are of the order of 1 kHz, which makes these gates slow. The first way to improve this is to use adiabatic passage, i.e., a sweep of the detuning across the resonance, which allows a single-qubit rotation of the order of the level spacing. Below, we discuss in more detail another scheme based on fast switching of the phase ϕ_0 of the Raman coupling Ω_{ab}.

Assume $H_A=\mathcal{H}_0(\phi_0=0.495)$, $H_B=\mathcal{H}_0(\phi_0=0.5)$, and $[H_A,H_B]\neq 0$. We know from group theory that by switch-

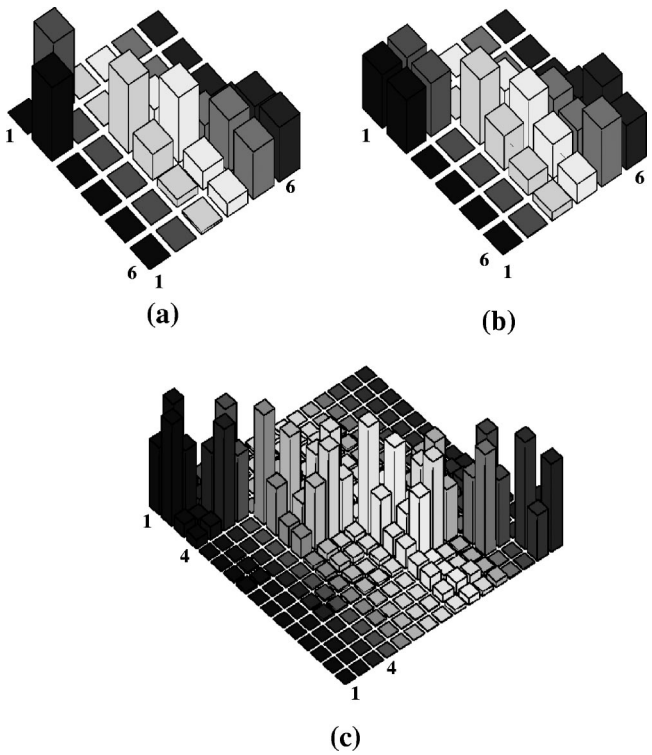

FIG. 5. The absolute value of the elements of the unitary transformations for quantum logic gates, $|U_{ij}|$. The transformations are on the lowest six states of the qubits with the lowest two states the $|\uparrow\rangle$ and $|\downarrow\rangle$ states of the qubit. (a) Single-qubit NOT gate. The labels indicate the lowest-qubit states from 1 to 6. (b) Single-qubit Hadamard gate. Labels are the same as in (a). (c) A two-qubit gate by a 36-pulse sequence. The labels 1–4 are the qubit states $|\uparrow\uparrow,\uparrow\downarrow,\downarrow\uparrow,\downarrow\downarrow\rangle$. The rest are higher states.

ing the phase alternatively between these two phase values, any desired unitary transformation can be constructed within a reasonable number of switchings as $U=e^{-iH_At_{2n}}e^{-iH_Bt_{2n-1}}\cdots e^{-iH_At_2}e^{-iH_Bt_1}$ by adjusting the durations t_i of the pulses [16]. For a single-qubit gate, we want the unitary transformation to be block diagonal between the two-qubit states and the other states. A numerical optimization of the $\{t_i\}$ is applied to a 12-pulse sequence of the H_A and H_B operators for the lowest six states of the qubit. We construct a NOT gate and a Hadamard gate U_H. The elements of the unitary operators $|U_{ij}|$ are shown in Figs. 5(a), and 5(b). The off-diagonal elements $U_{i,1},U_{i,2}\ll 0.005$ shows a high fidelity. The total time for the gates is $\tau_1\sim 2$ msec for both gates. The accuracy of the gate can be improved by increasing the number of pulses in the sequence while keeping the total gate time short (which means faster switching of the operators $H_{A,B}$).

Note that the above approach relies on the fast and accurate switching of the phase ϕ_0 of the lasers, which can be achieved experimentally with no difficulty.

The collision energy is the slowest-energy scale which limits the speed of the quantum logic gates, while the Raman couplings can be well controlled by lasers. In practice, Feshbach resonances can be exploited to adjust the scattering length by several orders of magnitude [17,18] and the gate speed can be improved.

B. Two-bit gate

Two-bit gates can be constructed by external Josephson tunneling between neighboring qubits in the optical lattice. As we mentioned earlier, external Josephson tunneling is the tunneling of atoms between spatially separated condensates. With the geometry in Fig. 2(a), where the qubits are aligned parallel along the longitudinal direction of the cigar-shaped trap, atoms can tunnel from one lattice site to its neighboring sites when the trapping potential of the optical lattice is lowered for short times. By decreasing the amplitude of the laser, the trapping potential can be decreased and the tunneling increases exponentially. The tunneling is also enhanced by a factor of N_t of the number of atoms.

We consider the tunneling interaction

$$\mathcal{H}_2=\Omega_t\sum_\alpha\,(a_{1\alpha}^\dagger a_{2\alpha}+a_{2\alpha}^\dagger a_{1\alpha}), \tag{7}$$

the indices 1 and 2 in the operators refer to qubits 1 and 2. The tunneling matrix can be estimated with the WKB approximation: $\Omega_t\sim(\omega_\perp/2\pi)\exp(-\Delta U/\hbar\omega_\perp)$, with $\omega_\perp$ being the plasma frequency of the atoms in the trapping potential and ΔU the trapping barrier for the qubit. The single-particle tunneling Ω_t is enhanced by the number of particles and so does the speed of two-bit logic gates. The tunneling rate can be controlled by adjusting the laser pulse.

The interaction $\mathcal{H}_2$ can be calculated numerically. The matrix elements of the operator $(a_\alpha^\dagger)_{ij}$ is obtained by calculating the overlap between the states $|i_{N_t+1}\rangle$ for N_t+1 atoms and the states $a_\alpha^\dagger|j_{N_t}\rangle$. Our calculation shows that this interaction as well as that of the single-qubit gate induces coupling to the higher states of the qubits. This problem can be prevented by the same approach as that of the single-qubit gate—fast-pulse sequence to decouple the lower states from the higher states. We apply a pulse sequence of 36 pulses with $H_A=\mathcal{H}_2(\phi_0)$ and $H_B=\mathcal{H}_0^{(1)}(\phi_0)+\mathcal{H}_0^{(2)}(\phi_0)$, where $\mathcal{H}_0^{(1,2)}$ are single-qubit Hamiltonian at ϕ_0. In Fig. 5(c), we show the absolute values of the matrix elements for a two-bit transformation at $\phi_0=0.5$. With a total pulse duration of 1 msec, the fidelity of the gates for $N_t=15$ atoms is higher than 98%.

V. ADIABATIC PROCESS AND MEASUREMENT

The qubit we studied in the previous sections works in the Josephson regime where $U_0N_t^2\gg\Omega_0N_t\gg U_0$. In this section, we present a projective measurement scheme during which the qubit is switched adiabatically between the Josephson regime and the Rabi regime where $\Omega_0N_t\gg U_0N_t^2$. In contrast to the measurement of solid-state qubit where it takes efforts to build efficient measurement schemes, our method provides an easy-to-realize way for qubit readout. The same approach can also be applied to initialize the qubit.

A. Qubit in the Rabi regime

In the Rabi regime, when the Josephson energy is much larger than the collision energy, we neglect the collision term and the qubit is described by the single-atom Hamiltonian

$$\mathcal{H}_J=-(a_1^\dagger,a_0^\dagger,a_{-1}^\dagger)\begin{pmatrix}0 & \Omega_0 & \Omega_1 e^{i\phi_0}\\ \Omega_0 & 0 & \Omega_0\\ \Omega_1 e^{-i\phi_0} & \Omega_0 & 0\end{pmatrix}\begin{pmatrix}a_1\\ a_0\\ a_{-1}\end{pmatrix}, \tag{8}$$

which describes a three-mode atom where the internal modes are coupled by lasers. The eigenstates can be described by atomic states as

$$\mathcal{H}_J=\sum_{i=1}^{3}\epsilon_i S_i^\dagger S_i, \tag{9}$$

where $S_i^\dagger$ and S_i are the operators for the atomic eigenstates and ϵ_i are the eigenenergies with $\epsilon_1<\epsilon_2<\epsilon_3$ and $2(\epsilon_2-\epsilon_1)<(\epsilon_3-\epsilon_1)$. The ground state and the lowest excited states of the qubit with N_t atoms can be described by the atomic states

$$|\psi_1^J\rangle=\frac{(S_1^\dagger)_t^N}{\sqrt{N_t!}}|0\rangle,\quad E_1^J=N_t\epsilon_1,$$

$$|\psi_2^J\rangle=\frac{S_2^\dagger(S_1^\dagger)^{N_t-1}}{\sqrt{(N_t-1)!}}|0\rangle,\quad E_2^J=(N_t-1)\epsilon_1+\epsilon_2, \tag{10}$$

$$|\psi_3^J\rangle=\frac{(S_2^\dagger)^2(S_1^\dagger)^{N_t-2}}{\sqrt{(N_t-2)!}}|0\rangle,\quad E_3^J=(N_t-2)\epsilon_1+2\epsilon_2,$$

where in the ground state $|\psi_1^J\rangle$, all atoms stay in the lowest atomic state $|S_1\rangle$. In the first excited state $|\psi_2^J\rangle$, one atom is excited to the $|S_2\rangle$ state and all the others stay in the lowest atomic state. This result is also confirmed by the numerical calculations.

When the collision term cannot be neglected, we numerically solve the Hamiltonian in Eq. (3). In Fig. 6(a), the calculated energies for the qubit for a large range of Ω_0 are plotted. The inset of this plot shows the persistent currents of qubit states versus Ω_0. The average currents $\langle I_{1,0}\rangle$ of the two-qubit states converge to each other as Ω_0 increases.

B. Initial-state preparation

When the Raman coupling Ω_0 is tuned slowly, the qubit state can be manipulated adiabatically. Here ''slow'' means

$$\left|\min_{\Omega_0}\{E_2(\Omega_0)-E_1(\Omega_0)\}\right|^2\gg\frac{d\Omega_0}{dt}, \tag{11}$$

where $d\Omega_0/dt$ is how fast Ω_0 is tuned, and $\min_{\Omega_0}\{E_2(\Omega_0)-E_1(\Omega_0)\}$ is the smallest energy difference between the qubit states during the tuning process. As is shown in Fig. 6(a), it reaches its minimum at the leftmost end when Ω_0 is small. Hence the switching process takes a time of milliseconds.

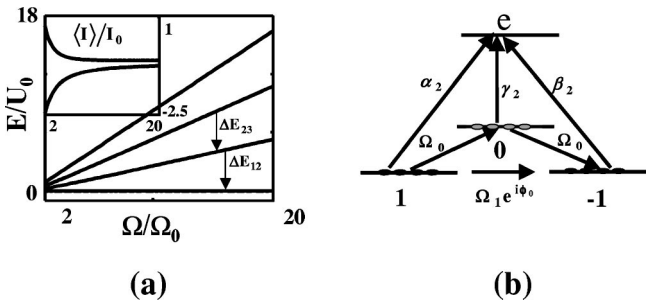

FIG. 6. Adiabatic switching of Raman tunnelings. (a) The energy spectrum of the qubit vs the Raman coupling Ω. The Raman coupling is plotted in units of the Raman coupling Ω_0 for the designed qubit. The energy differences between states ΔE_{12} and ΔE_{23} are indicated by arrows. The inset shows the average current $\langle I\rangle/\Omega$ in the same range of Ω. (b) The laser pulse $\mathcal{H}_m$ of the projective measurement after the adiabatic switching. The coupling constants α_2, β_2, and γ_2 show the relative phase between the three components of the pulse.

This adiabatic process can be exploited for efficiently initializing the qubit to its ground state. Starting from the large Ω_0 limit, we prepare the qubit in its ground state $|\psi_1^J\rangle$, which is equivalent to preparing all the atoms in state $|S_1\rangle$ and which can be achieved easily. Then, the Raman coupling is adiabatically decreased to the working regime so that the ground state $|\psi_0^q\rangle$ is reached with high fidelity.

C. Projective measurement

Second, and most important, the adiabatic switching provides a scheme for a projective measurement of the qubit. Starting from the working parameters of the qubit where $2\Omega_0 N_t/U_0=210$ and assuming an initial state $\alpha|\psi_0^q\rangle+\beta|\psi_1^q\rangle$, Ω_0 is slowly increased to the Rabi regime. When $\Omega_0 N_t\gg U_0$, the qubit state evolves to $\alpha|\psi_1^J\rangle+\beta|\psi_2^J\rangle$, a superposition of the states in Eq. (10). As the increase of Ω_0 is adiabatic, no transition to the excited state is induced. Then, a dark-state measurement scheme is performed on the qubit, that is, a laser pulse is applied which excites the atomic state $|S_2\rangle$ to an excited state $|e\rangle$ and does nothing to the atoms in the states $|S_1\rangle$ and $|S_3\rangle$. The state $|e\rangle$ emits a photon via spontaneous emission which is then detected. As can be seen from Eq. (10), when the laser is applied to the ground state $|\psi_1^J\rangle$, no transition occurs and no photon is emitted; when the laser is applied to the second state $|\psi_2^J\rangle$, one atom is excited to the state $|e\rangle$ and one photon is emitted. Hence, this approach achieves a projective measurement of the qubit.

The laser pulse applied after the adiabatic switching is

$$\mathcal{H}_m=e^\dagger S_2+S_2^\dagger e, \tag{12}$$

where $e^\dagger$ and e are the operators for the excited state $|e\rangle$. It is easy to prove that single-atom states S_1 and S_3 are dark states of this operator which cannot be excited by this pulse [as they are orthogonal states of the Hamiltonian in Eq. (8)]. We have $\mathcal{H}_m|\psi_1^J\rangle=0$ and $\mathcal{H}_m|\psi_1^J\rangle=|(N-1)_{S_1},1_e\rangle$. By performing a single-photon measurement with the quantum

jump approach, the probability of the qubit in $|\psi_1^J\rangle$, and hence in $|\psi_1^q\rangle$ originally, can be detected.

VI. DECOHERENCE

A major obstacle in pursuing quantum computation with solid-state qubits is the strong coupling to noise and the resulting low quality factor. In experiment, the measured decoherence time for the superconducting qubits is $T_2 = 100$ nsec, while the gate time is $\tau_{gate} = 10$ nsec [8].

In the atomic qubit presented in this paper, the quality factor due to decoherence is is higher compared with that of the superconducting qubit. The qubit is designed to be insensitive to the major factors that can result in decoherence. For example, all the energies involved in qubit operation are much lower than the trapping frequency in the longitudinal direction of the trap $\omega_{\|} = 3.7$ kHz, which keeps the atoms in the motional ground state during gate operations. Other factors such as the inaccuracy in the Raman couplings, the particle loss from the trap, and the spontaneous emissions can be well neglected within a time of seconds.

The fluctuation of the number of atoms could induce severe qubit decoherence when the number of atoms is large. For example, the decoherence rate due to single-particle loss grows linearly with N_t and the decoherence rate due to three-body collision increases with N_t^3. Our study shows that for the single-particle loss process with coupling constant γ_0, the decoherence rate at $N_t = 15$ is $1.6\gamma_0$ and the decoherence due to three-body collision can be neglected.

A. Effect of single-atom loss

Consider, for example, a single-atom loss characterized by a loss rate γ. The time evolution of the density matrix is described by the following master equation:

$$\frac{\partial \rho^t}{\partial t} = -i[\mathcal{H}_I(t), \rho^t],$$

$$\frac{\partial \rho^t}{\partial t} = -\gamma_0 \sum_\alpha (\hat{a}_\alpha^\dagger \hat{a}_\alpha \rho^t + \rho^t \hat{a}_\alpha^\dagger \hat{a}_\alpha - 2\hat{a}_\alpha \rho^t \hat{a}_\alpha^\dagger), \qquad (13)$$

where ρ^t is the density matrix of the qubit in the interaction picture and the atomic losses in different modes are summed up.

The density matrix can be decomposed into the Hilbert spaces of different numbers of atoms: $\rho^t = \Sigma_n \rho_{ij}^{(n)} |i_n\rangle\langle j_n|$, where $\rho_{ij}^{(n)} = \langle i_n|\rho^t|j_n\rangle$ is the element of the density matrix with n atoms and $|i_n, j_n\rangle$ are qubit states of n atoms. Substituting this expression into Eq. (13) and assuming an initial density matrix ρ^0 with N_t atoms, we have

$$\rho_{ij}^{eff}(\delta t) = \rho_{ij}^{(N_t)} + \rho_{ij}^{(N_t-1)},$$

$$\rho^{(N_t)} = \rho^0 - \delta t \gamma_0 \sum_\alpha A_\alpha^\dagger A_\alpha \rho^0 + \rho^0 A_\alpha^\dagger A_\alpha, \qquad (14)$$

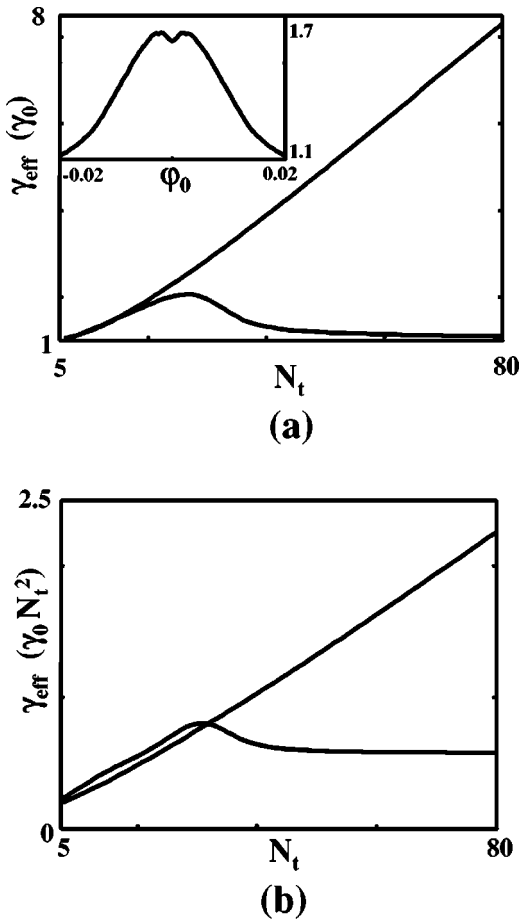

FIG. 7. Decoherence rate by Eq. (15). (a) Single-atom loss rate vs number of atoms. Upper curve, $\phi_0 = 0.5$; and lower curve, $\phi_0 = 0.495$. Inset: single-atom loss rate vs the phase ϕ_0 at $N_t = 15$. (b) Three-body loss rate units of $\gamma_0 N_t^2$ vs the number of atoms. Upper curve, $\phi_0 = 0.5$; and lower curve, $\phi_0 = 0.495$.

$$\rho^{(N_t-1)} = +2\,\delta t \gamma_0 \sum_\alpha A_\alpha \rho^0 A_\alpha^\dagger,$$

where the matrix $(A_\alpha^\dagger)_{ij} = \langle i_{N_t}|\hat{a}_\alpha^\dagger|j_{N_t-1}\rangle$. Starting from N_t atoms in the trap, when one atom leaks out, the qubit state is a superposition of the eigenstates of (N_t-1) atoms. The decoherence rate is slowed down by the fact that the remaining system of (N_t-1) atoms largely overlaps with the original qubit states in the (N_t-1)-atom basis. The decoherence rate is expressed as

$$\gamma_{\text{eff}} = \gamma_0 \max_{|\Psi\rangle} \left\{ \sum \langle\Psi|A_\alpha^\dagger A_\alpha|\Psi\rangle - |\langle\Psi|A_\alpha^\dagger|\Psi\rangle|^2 \right\}, \qquad (15)$$

where the maximum is derived for any $|\Psi\rangle$ in the Hilbert space of the qubit.

In Fig. 7(a), we plot γ_{eff} versus N_t at $\phi_0 = 0.5$ and 0.495, which grows linearly when N_t is not very large. At $N_t = 15$, $\gamma^{eff} = 1.6\gamma_0$. As N_t increases, γ_{eff} at $\phi_0 = 0.495$ becomes saturated, while γ_{eff} at $\phi_0 = 0.5$ keeps increasing linearly with N_t. In the inset of Fig. 7(a), we plot the dependence of

the decoherence rate on the phase ϕ_0 at $N_t=15$, which does not vary strongly with ϕ_0 in the range of interest.

B. Three-body collision loss

One of the main decoherences against this qubit is the three-body collision loss. The three-body process $A+A+A \rightarrow A_2+A$ describes that when three atoms collide, two atoms form a bounded molecular state with a binding energy of the order of $\hbar^2/ma_s^2$, which is several orders larger than the trapping frequency, where a_s is the *s*-wave scattering length. As a result, the molecule and atom gain very large kinetic energy after the collision and escape from the trap. This process damages the coherence of the qubit states. The dynamics of the qubit is still described by Eq. (15), with γ_0 replaced by the three-body loss rate $\gamma_0^{(3)}=K_3(8\rho)^2/72(3\pi^2)^{3/2}N_t^2$, where K_3 is the three-body collision rate in Refs. [19,20] and $\int d^3\vec{x}|\psi(\vec{x})|^6$ gives the dependence on the density and on the number of atoms, and the operator A_α replaced by A_α^3. We apply the same approach as that for the single-atom loss to calculate the effective decoherence rate and the results are plotted in Fig. 7(b). It is shown that $\gamma_{\rm eff}/\gamma_0^{(3)}N_t^2$ grows linearly with N_t at small N_t, and at $N_t=15$, $\gamma_{\rm eff}\approx 0.5\gamma_0^{(3)}N_t^2$. With $\rho=3\times10^{14}$ cm^{-3} and $K_3=10^{-28}$ cm^6/sec, we have $\gamma_{\rm eff}=0.02$, which gives a small decoherence rate.

VII. CONCLUSIONS

We have presented a scheme for implementing an atomic flux qubit with atomic Josephson junctions, which are generated by Raman lasers that introduce coupling between internal modes of atoms. By trapping three internal modes and coupling them with the Raman pulse, a three-junction loop is constructed. The collision interaction between the atoms provides the analog of the capacitance energy. With a small number of atoms, the qubit presents the main features of the mesoscopic circuit—superconducting flux qubit: the butterfly shaped energy spectrum, the persistent currents, and the local wave function in phase basis. We have outlined methods for the implementation of quantum logic gates with fast switching of Raman pulses, the state initialization, and we have presented a projective measurement scheme by adiabatic switching of the Josephson coupling and observation of quantum jumps. Furthermore, we have given a detailed analysis of possible imperfection and decoherence of the qubit.

The solid-state qubits suffer severely from noise, which may become the biggest obstacle in implementing those qubits. However, the solid-state proposals are easy to scale up and control with existing technology. The qubit proposed in this paper inherits many of the merits of the superconducting qubits. For one thing, almost all the parameters of the qubit can be very well controlled by external sources, which increases the flexibility of qubit. The system is, in principle, scalable by storing the atomic flux qubit in wells of the 1D optical lattice. Compared with superconducting qubit, the atomic Josephson junction qubit has the advantage of not subjecting to severe environmental disturbance and having a long decoherence time. Hence, an array of the atomic qubits can be arranged in a space to simulate a ''clean'' array of superconducting qubits and perform certain quantum gate operations. Clearly, one of the main differences to the superconducting case is the significantly slower time scale of operations.

In summary, our study shows that the atomic systems can be designed to be a clean realization of the Josephson junction circuits and keep the merits of exploring macroscopic/mesoscopic degrees of freedom and a long decoherence time. In this system, the Josephson couplings can be controlled with large flexibility by adjusting the power and phases of the laser beams. The collision interaction can also be adjusted to a large extent by magneto-optical means such as tuning around the Feshbach resonances [21]. Moreover, the trap geometry and the interaction between neighboring qubits can be chosen to suit different experiments.

ACKNOWLEDGMENTS

We would like to thank J. I. Cirac for helpful discussions. Work at the University of Innsbruck was supported by the Austrian Science Foundation, European Networks, and the Institute for Quantum Information.

[1] M. Tinkham, *Introduction to Superconductivity*, 2nd ed. (McGraw-Hill, New York, 1996).

[2] T. P. Orlando and K. A. Delin, *Introduction to Applied Superconductivity* (Addison-Wesley, Reading, MA, 1991).

[3] A.J. Leggett, Rev. Mod. Phys. **73**, 307 (2001).

[4] D.S. Hall *et al.*, Phys. Rev. Lett. **81**, 1543 (1998); S. Inouye *et al.*, Nature (London) **392**, 15 (1998); W.M. Liu, W.B. Fan, W.M. Zheng, J.Q. Liang, and S.T. Chui, Phys. Rev. Lett. **88**, 170408 (2002).

[5] J. Javanainen, Phys. Rev. Lett. **57**, 3164 (1986); I. Zapata, F. Sols, and A.J. Leggett, Phys. Rev. A **57**, R28 (1998); J. Ruostekoski *et al.*, *ibid.* **57**, 511 (1998); E.L. Bolda, S.M. Tan, and D.F. Walls, Phys. Rev. Lett. **79**, 4719 (1997); R. Walser, *ibid.* **79**, 4724 (1997); A. Smerzi, S. Fantoni, S. Giovanazzi, and S.R. Shenoy, *ibid.* **79**, 4950 (1997); S. Giovanazzi, A. Smerzi, and S. Fantoni, *ibid.* **84**, 4521 (2000); S. Raghavan, A. Smerzi, S. Fantoni, and S.R. Shenoy, Phys. Rev. A **59**, 620 (1999); J.R. Anglin, P. Drummond, and A. Smerzi, *ibid.* **64**, 063605 (2001); J.R. Anglin and A. Vardi, *ibid.* **64**, 013605 (2001).

[6] Y. Makhlin, G. Schön, and A. Shnirman, Rev. Mod. Phys. **73**, 357 (2001).

[7] J.E. Mooij, T.P. Orlando, L. Levitov, Lin Tian, Caspar H. van der Wal, and Seth Lloyd, Science **285**, 1036 (1999).

[8] T.P. Orlando, J.E. Mooij, Lin Tian, Caspar H. van der Wal, L. Levitov, Seth Lloyd, and J.J. Mazo, Phys. Rev. B **60**, 15 398 (1999).

[9] I. Chiorescu, Y. Nakamura, C.J.P.M. Harmans, and J.E. Mooij, Science **299**, 1869 (2003).

[10] K. Schulze, Diploma thesis, University of Innsbruck, 1999.
[11] J.J. García-Ripoll and J.I. Cirac, Phys. Rev. Lett. **90**, 127902 (2003); note that small fluctuation of the number of atoms does not affect our discussions on the qubit.
[12] D.P. DiVincenzo, Fortschr. Phys. **48**, 769 (2000), special issue on experimental proposals for quantum computation; e-print quant-ph/0002077.
[13] Tin-Lun Ho, Phys. Rev. Lett. **81**, 742 (1998).
[14] C.K. Law, H. Pu, and N.P. Bigelow, Phys. Rev. Lett. **81**, 5257 (1998).
[15] The term $\hat{a}_1^\dagger \hat{a}_{-1}^\dagger \hat{a}_0^2$ can be suppressed by shifting the atomic levels by external fields, so that energy conservation in the collision is violated, i.e., these terms average away in the Hamiltonian. Note that in our numerical calculations, we include this term to count for the exact form of the interaction.
[16] S. Lloyd, Phys. Rev. Lett. **75**, 346 (1995).
[17] F.A. van Abeelen and B.J. Verhaar, Phys. Rev. A **59**, 578 (1999).
[18] E.R.I. Abraham, W.I. McAlexander, J.M. Gerton, R.G. Hulet, R. Cote, and A. Dalgarno, Phys. Rev. A **55**, R3299 (1997).
[19] B.D. Esry, Chris H. Greene, and James P. Burke, Jr., Phys. Rev. Lett. **83**, 1751 (1999).
[20] M.W. Jack, Phys. Rev. Lett. **89**, 140402 (2002).
[21] A.J. Moerdijk, W.C. Stwalley, R.G. Hulet, and B.J. Verhaar, Phys. Rev. Lett. **72**, 40 (1994); A.J. Moerdijk and B.J. Verhaar, *ibid.* **73**, 518 (1994); A.J. Moerdijk, B.J. Verhaar, and A. Axelsson, Phys. Rev. A **51**, 4852 (1995).